

## Supporting Information

### **In Situ Derived Fe/N/S-Codoped Carbon Nanotubes from ZIF-8 Crystals as Efficient Electrocatalysts for Oxygen Reduction Reaction and Zinc-Air Batteries**

Huihui Jin<sup>a</sup>, Huang Zhou<sup>a</sup>, Wenqiang Li<sup>a</sup>, Zhihao Wang<sup>a,b</sup>, Jinlong Yang<sup>a</sup>, Yuli Xiong<sup>c</sup>, Daping He<sup>a,b\*</sup>, Lei Chen<sup>a\*</sup>, Shichun Mu<sup>a\*</sup>

<sup>a</sup> *State Key Laboratory of Advanced Technology for Materials Synthesis and Processing,*

*Wuhan University of Technology, Wuhan 430070, China*

<sup>b</sup> *Hubei Engineering Research Center of RF-Microwave Technology and Application, Wuhan*

*University of Technology, Wuhan 430070, China*

<sup>c</sup> *Michael Grätzel Center for Mesoscopic Solar Cells (MGC), Wuhan National Laboratory for*

*Optoelectronics, School of Optical and Electronic Information, Huazhong University of Science*

*and Technology, Wuhan 430074, China*

*E-mail: [hedaping@whut.edu.cn](mailto:hedaping@whut.edu.cn), [CHL0583@163.com](mailto:CHL0583@163.com), [msc@whut.edu.cn](mailto:msc@whut.edu.cn)*

**RDE and RRDE technique**

In RDE testing, the electron transfer number was calculated by Koutecky-Levich equation:

$$\frac{1}{j} = \frac{1}{j_L} + \frac{1}{j_K} = \frac{1}{B\omega^{1/2}} + \frac{1}{j_K}$$

$$B = 0.62nFC_0D^{2/3}\nu^{-1/6}$$

Where  $j$  is the measured current density,  $j_K$  is the kinetic current density,  $j_L$  is the limiting current density,  $\omega$  is the angular velocity of the electrode rotation,  $n$  is the electron transfer number,  $F$  is the Faraday constant (96485 C/mol),  $C_0$  is the bulk concentration of  $O_2$  ( $1.2 \times 10^{-6}$  mol/cm<sup>3</sup> for 0.1 M KOH,  $1.1 \times 10^{-6}$  mol/cm<sup>3</sup> for 0.5 M H<sub>2</sub>SO<sub>4</sub>),  $D$  is the diffusion coefficient of  $O_2$  ( $1.9 \times 10^{-5}$  cm<sup>2</sup>/s<sup>1</sup> in 0.1 M KOH,  $1.8 \times 10^{-5}$  cm<sup>2</sup>/s<sup>1</sup> in 0.5 M H<sub>2</sub>SO<sub>4</sub>), and  $\nu$  is the kinematic viscosity of the electrolyte (0.01 cm<sup>2</sup>/s<sup>1</sup> for both 0.1 M KOH and 0.5 M H<sub>2</sub>SO<sub>4</sub> solution).

In RDDE testing, the electron transfer number and H<sub>2</sub>O<sub>2</sub>% yield were calculated by the following equation:

$$n = \frac{4I_d}{I_r + \frac{I_r}{N}}$$

$$H_2O_2\% = 200 \times \frac{\frac{I_r}{N}}{\frac{I_r}{N} + I_d}$$

Where the  $I_d$  is the disk current,  $I_r$  is the ring current,  $N=0.37$

### DFT Computation Details

Geometric optimization and total energy calculations were performed within DFT framework as implemented with DMol3 code. Spin-polarization was considered in all calculations. PBE exchange-correlation functional within the generalized gradient approximation (GGA) was

adopted. The all-electron-relativistic-core method was implemented to treat the relativistic effects. A double numerical basis set was used together with polarization functions (DNP). A smearing of 0.005 Ha (1 Ha = 27.21 eV) to the orbital occupation is applied to achieve accurate electronic convergence. Self-consistent-field (SCF) procedures were performed with a convergence criterion of  $1 \times 10^{-6}$  Ha on the total energy. The convergence tolerance of energy, force and displacement were 0.002 Ha/Å,  $1 \times 10^{-5}$  Ha, and 0.005 Å respectively in the geometry optimization. Periodical supercells containing single-layer graphenes with 20 Å vacuum above were used to model various graphene doping structures. The  $4 \times 4 \times 1$  Monkhorst–Pack grid k-points were employed to sample the Brillouin zone integration.

## Supplementary Figures and Tables

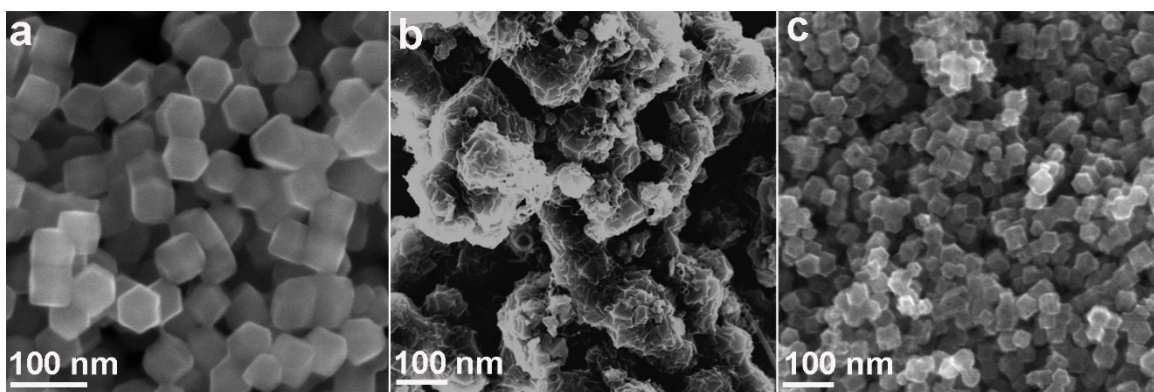


**Figure S1** SEM images of (a) ZIF-8, (b) Fe/N/S-C and (c) N-C.

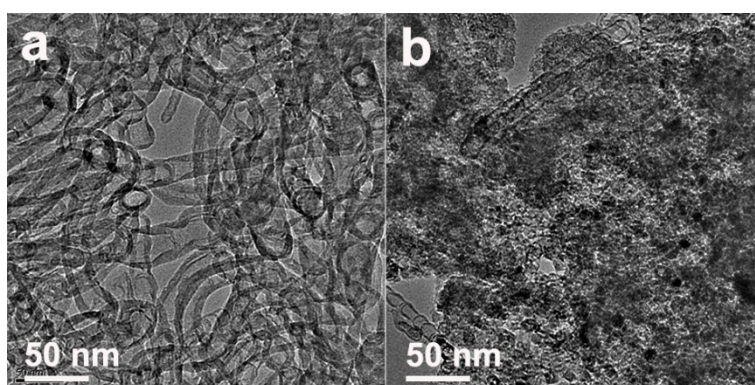


**Figure S2** TEM image of (a) Fe/N/S-CNTs and (b) Fe/N/S-C.

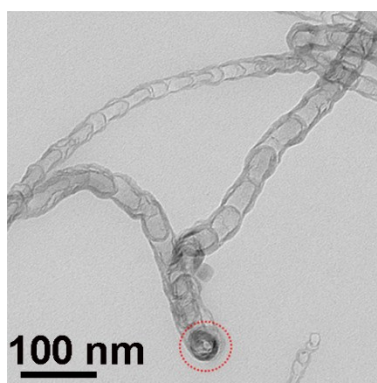


**Figure S3** TEM image of Fe/N/S-CNTs before acid etching.

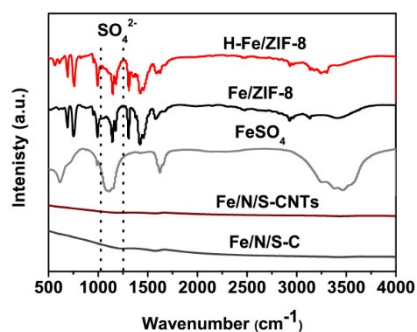


**Figure S4** FTIR spectra of precursors before (H-Fe/ZIF-8, Fe/ZIF-8 and FeSO<sub>4</sub>) and after pyrolysis (Fe/N/S-C and Fe/N/S-CNTs).

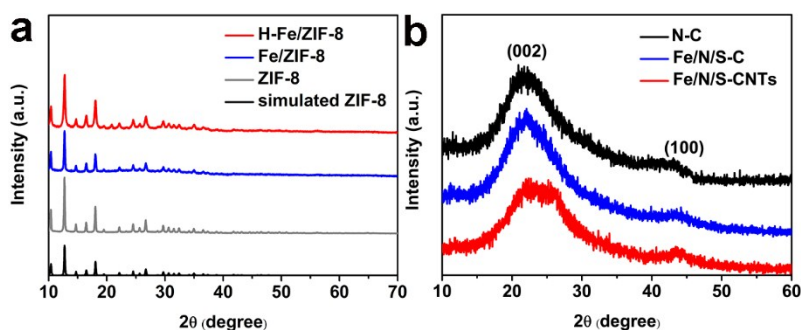


**Figure S5** XRD patterns of (a) precursors before pyrolysis, (b) carbides after pyrolysis.

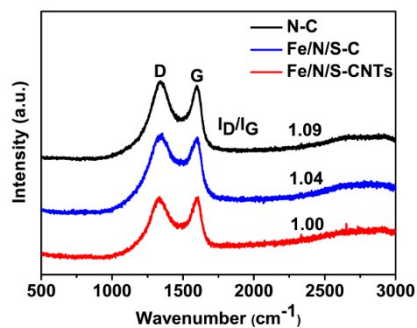


**Figure S6** Raman spectra of N-C, Fe/N/S-C and Fe/N/S-CNTs.

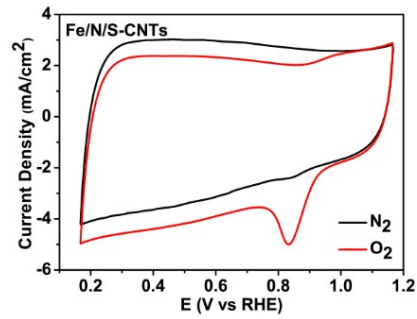


**Figure S7** CV curves of Fe/N/S-CNTs in 0.1 M KOH.

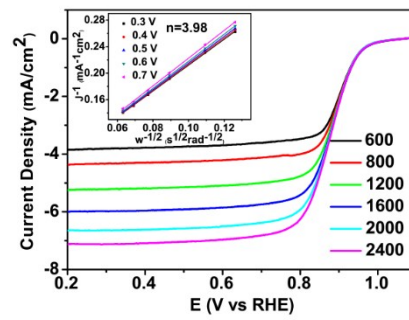


**Figure S8** LSV curves of Fe/N/S-CNTs at various rotation rates in 0.1 M KOH (inset: corresponding Koutecky-Levich plots).

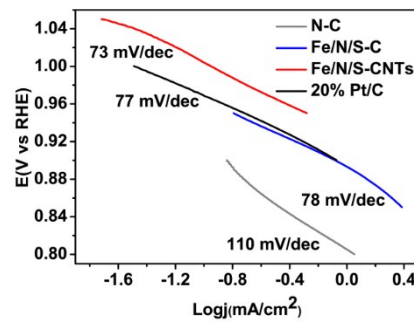


**Figure S9** Tafel slopes of N-C, Fe/N/S-C, Fe/N/S-CNTs and Pt/C in 0.1 M KOH.

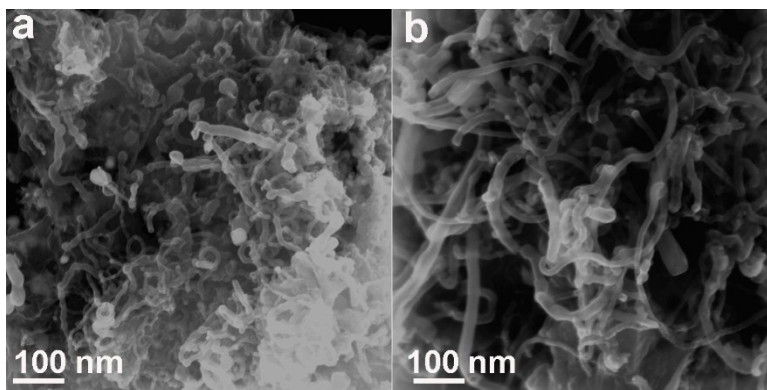


**Figure S10** SEM images of (a) Fe/N/S-CNTs-3 mL and (b) Fe/N/S-CNTs-9 mL

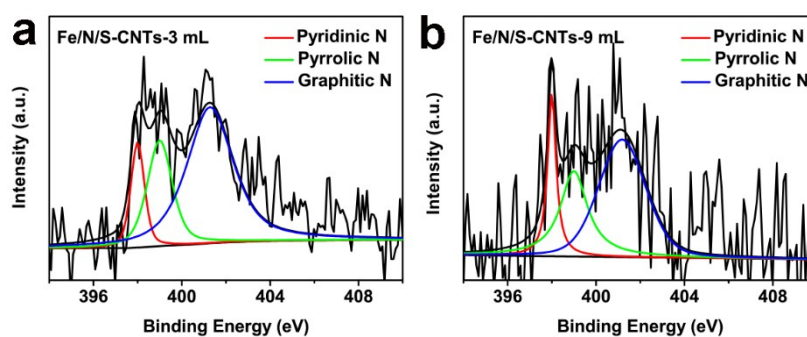


**Figure S11** N1s XPS spectra of (a) Fe/N/S-CNTs-3 mL and (b) Fe/N/S-CNTs-9 mL

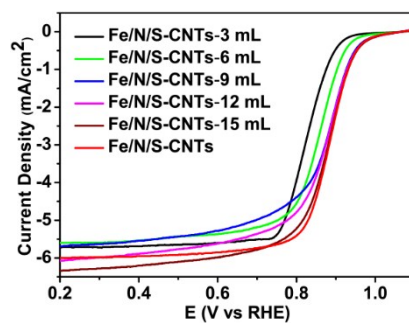


**Figure S12** LSV curves of the pyrolysis samples with different amount of hydrazine hydrate pretreatment.

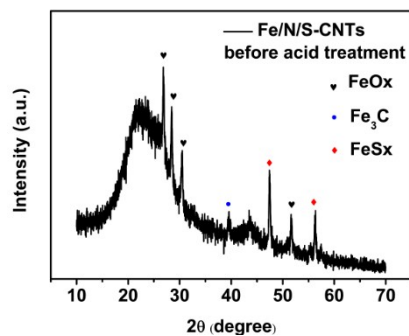


**Figure S13** XRD pattern of Fe/N/S-CNTs before acid treatment.

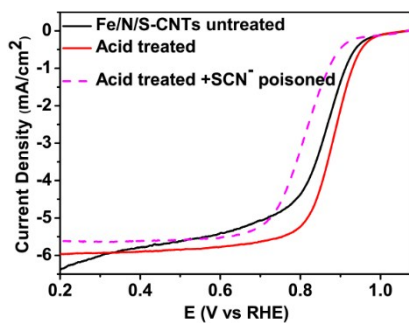


**Figure S14** LSV curves of Fe/N/S-CNTs before and after acid treatment and  $\text{SCN}^-$  poisoning.

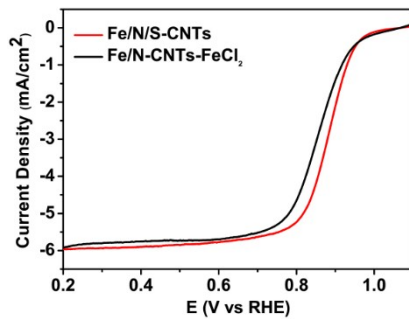


**Figure S15** LSV curves of the pyrolysis samples with different iron sources.

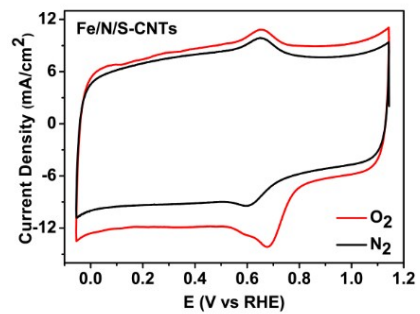


**Figure S16** CV curves of Fe/N/S-CNTs in 0.5 M H<sub>2</sub>SO<sub>4</sub>.

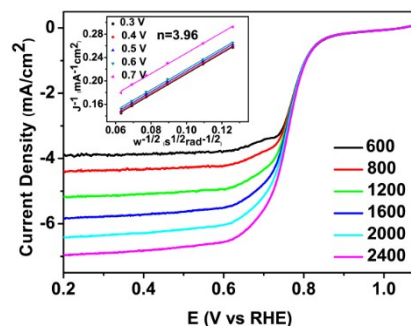


**Figure S17** LSV curves of Fe/N/S-CNTs at various rotation rates in 0.5 M H<sub>2</sub>SO<sub>4</sub> (inset: corresponding Koutecky–Levich plots).

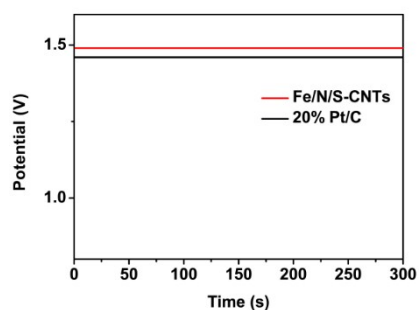


**Figure S18** Open-circuit potential of Fe/N/S-CNTs and Pt/C.

**Table S1.** Elements content of Fe/N/S-C and Fe/N/S-CNTs from element analyzer and ICP, and superficial surface atomic content from XPS peak table.

catalyst	C	N	S	Fe	Surface N	Surface Fe
	(wt %)	(wt %)	(wt %)	(wt %)	(Atomic %)	(Atomic %)
Fe/N/S-C	67.67	5.63	0.808	1.59	3.01	0.51
Fe/N/S-CNTs	68.8	5.34	1.051	1.43	6.21	0.59

**Table S2.** Comparison of the onset and half-wave potentials for ORR of non-noble metal catalysts systems from literature and this work in alkaline and acid medium

Catalyst	Electrolyte	$E_{1/2}$ vs RHE	Electrolyte	$E_{1/2}$ vs RHE	Reference
Fe/N/S-CNTs	0.1M KOH	0.887	0.5M H <sub>2</sub> SO <sub>4</sub>	0.767	This work
NCNTs-2.5	0.1M KOH	0.789	0.5M H <sub>2</sub> SO <sub>4</sub>		1
Fe@Fe <sub>3</sub> C/C-N	0.1M KOH	0.75	0.5M H <sub>2</sub> SO <sub>4</sub>	0.62	2
SN-CNTs	0.1M KOH	0.79	0.1M HClO <sub>4</sub>	0.56	3
Fe <sub>3</sub> /C	0.1M KOH	0.83	0.5M H <sub>2</sub> SO <sub>4</sub>	0.73	4
CoP-CMP800	0.1M KOH	0.82	0.5M H <sub>2</sub> SO <sub>4</sub>	0.64	5
PCN-FeCo/C	0.1M KOH	0.85	0.5M H <sub>2</sub> SO <sub>4</sub>	0.76	6
BCNFNHs	0.1M KOH	0.861	0.5M H <sub>2</sub> SO <sub>4</sub>	0.65	7
NFe/CNs	0.1M KOH	0.859	0.5M H <sub>2</sub> SO <sub>4</sub>		8
5%Fe-N/C	0.1M KOH		0.5M H <sub>2</sub> SO <sub>4</sub>	0.735	9
MSZIF-900	0.1M KOH	0.84	0.5M H <sub>2</sub> SO <sub>4</sub>	0.72	10

## References

- 1 P. Su, H. Xiao, J. Zhao, Y. Yao, Z. Shao, C. Li, Q. Yang, Chem. Sci, **2013**,4, 2941-2946.
- 2 K. Ai, Y. Liu, C. Ruan, L. Lu, G.M. Lu, Adv. Mater, **2013**, 25,998-1003.
- 3 Q. Shi, F. Peng, S. Liao, H. Wang, H. Yu, Z. Liu, B. Zhang, D. Su, J. Mater. Chem. A, **2013**, 1, 14853-14857.
- 4 Y. Hu, J. Jensen, W. Zhang, L. Cleemann, W. Xing, N. Bjerrum, Q. Li, Angew. Chem. Int. Ed, **2014**, 53, 3749-3749.
- 5 Z.S. Wu, L. Chen, J. Liu, K. Parvez, H. Liang, J. Shu, H. Sachdev, R. Graf, X. Feng, K. Müllen, Adv. Mater, **2014**, 26, 1450-1455.

- 6 Q. Lin, X. Bu, A. Kong, C. Mao, F. Bu, P. Feng, *Adv. Mater*, **2015**, 27, 3431-3436.
- 7 W. Yang, X. Liu, X. Yue, J. Jia, S. Guo, *J. Am. Chem. Soc*, **2015**, 137, 1436.
- 8 S. Li, C. Cheng, H. Liang, X. Feng, A. Thomas, *Adv. Mater*, **2017**, 1700707.
- 9 Q. Lai, L. Zheng, Y. Liang, J. He, J. Zhao, J. Chen, *ACS Catal*, **2017**, 7, 1655-1663.
- 10 G. Jia, W. Zhang, G. Fan, Z. Li, D. Fu, W. Hao, C. Yuan, Z. Zou, *Angew. Chem. Int. Ed*, **2017**, 56, 13781-13785.